

# Isomorphous Insertion of Ce(III)/Ce(IV) Centers into Layered Double Hydroxide as a Heterogeneous Multifunctional Catalyst for Efficient Meerwein–Ponndorf–Verley Reduction

Gábor Varga,\* Thanh-Truc Nguyen, Jing Wang, Dihua Tian, Run Zhang, Li Li, and Zhi Ping Xu\*



Cite This: *ACS Appl. Mater. Interfaces* 2024, 16, 11453–11466



Read Online

ACCESS |

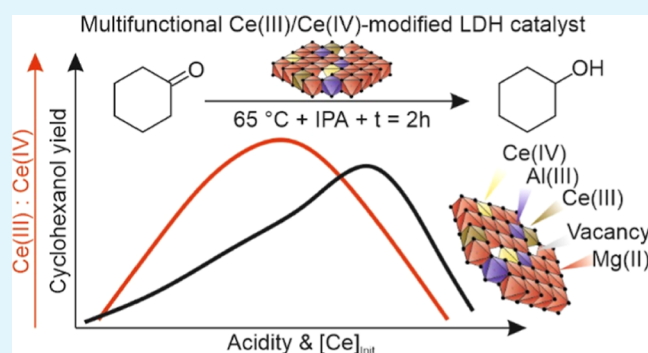
Metrics & More

Article Recommendations

Supporting Information

**ABSTRACT:** The development of highly active acid–base catalysts for transfer hydrogenations of biomass derived carbonyl compounds is a pressing challenge. Solid frustrated Lewis pairs (FLP) catalysis is possibly a solution, but the development of this concept is still at a very early stage. Herein, stable, phase-pure, crystalline hydrotalcite-like compounds were synthesized by incorporating cerium cations into layered double hydroxide (MgAlCe-LDH). Besides the insertion of well-isolated cerium centers surrounded by hydroxyl groups, the formation of hydroxyl vacancies near the aluminum centers, which were formed by the insertion of cerium centers into the layered double hydroxides (LDH) lattice, was also identified. Depending on the initial cerium concentration, LDHs with different Ce(III)/Ce(IV) ratios were produced, which had Lewis acidic and basic characters, respectively. However, the acid–base character of these LDHs was related to the actual Ce(III)/Ce(IV) molar ratios, resulting in significant differences in their catalytic performance. The as-prepared structures enabled varying degrees of transfer hydrogenation (Meerwein–Ponndorf–Verley MPV reduction) of biomass-derived carbonyl compounds to the corresponding alcohols without the collapse of the original lamellar structure of the LDH. The catalytic markers through the test reactions were changed as a function of the amount of Ce(III) centers, indicating the active role of Ce(III)–OH units. However, the cooperative interplay between the active sites of Ce(III)-containing specimens and the hydroxyl vacancies was necessary to maximize catalytic efficiency, pointing out that Ce-containing LDH is a potentially commercial solid FLP catalysts. Furthermore, the crucial role of the surface hydroxyl groups in the MPV reactions and the negative impact of the interlamellar water molecules on the catalytic activity of MgAlCe-LDH were demonstrated. These solid FLP-like catalysts exhibited excellent catalytic performance (cyclohexanol yield of 45%; furfuryl alcohol yield of 51%), which is competitive to the benchmark Sn- and Zr-containing zeolite catalysts, under mild reaction conditions, especially at low temperature ( $T = 65\text{ }^{\circ}\text{C}$ ).

**KEYWORDS:** transfer hydrogenation, solid frustrated Lewis pairs catalysts, layered double hydroxides, isomorphous substitution, Ce(III)/Ce(IV) insertion, cyclohexanone reduction



## INTRODUCTION

Both the reduction of carbonyl compounds<sup>1</sup> and the oxidation (dehydrogenation) of alcohols,<sup>2</sup> especially secondary alcohols, are of particular importance from an industrial point of view. Although there are well-established processes for carrying out these basic conversions, these conversions suffer greatly from being time-consuming, wasteful, and requiring isolation/purification steps to remove undesired products and by-products.<sup>1,2</sup> These aspects are far from the requirements of green chemistry,<sup>3</sup> and the emerging demand to optimize the redox economy of the synthesis processes, i.e., to minimize the number of oxidation state changes throughout the process,<sup>4</sup> has led to the golden age of catalytic transfer hydrogenations (CTHs).<sup>5,6</sup> Recently, this trend has been further strengthened as CTH reactions play a key role in many catalytic reaction cascades for the conversion of biomass-derived molecules into

valuable products, which can greatly contribute to achieving the main goals of the circular economy.<sup>7–13</sup>

CTHs enable easy-to-use, affordable carbonyl reductions as well as alcohol oxidations even if in one-pot reactions.<sup>5,7</sup> Moreover, they offer many advantages, from their well-controlled selectivity, including stereoselectivity (asymmetric transfer hydrogenations), and waste-minimized/time-spare features to the fact that they can be easily performed with

**Received:** November 8, 2023

**Revised:** February 8, 2024

**Accepted:** February 13, 2024

**Published:** February 26, 2024



heterogeneous catalytic processes, which increases their competitiveness.<sup>5,7</sup> From a mechanistic point of view, two different types of intermolecular CTHs has been distinguished, i.e., the metal hydride route<sup>14</sup> and the direct hydrogen transfer route.<sup>15</sup> When the direct hydrogen transfer takes place between the  $\alpha$ -H of the alcohol, which serves as the hydrogen source, and the carbonyl carbon via the formation of a six-membered-ring intermediate, this type of transfer hydrogenations is generally referred to as the Meerwein–Ponndorf–Verley (MPV) reduction.<sup>7,15</sup> In heterogeneous catalysis, processes that follows this latter mechanism are proved to be even more useful than other transfer hydrogenation strategies.<sup>5,7,15</sup> MPV catalysts typically have bifunctional features, particularly an acid–base character.<sup>7,16</sup> In the homogeneous phase, Lewis alkoxides with electron-deficient metal centers [i.e., Al(*i*-Pro)<sub>3</sub> or Ti(*i*-Pro)<sub>3</sub>] play the role of the promoter.<sup>16</sup> It is noteworthy that both Lewis acid and base sites promote MPV, their coexistence being sufficient.<sup>5,7,16</sup>

Despite all the desirable progresses made, homogeneous catalysts have possessed considerable disadvantages due to the difficulties of ligand exchange, making the use of ligand excess sufficient, the separation of the catalysts from the products, and their sensitivity to water.<sup>17</sup> There is therefore a notable need to find viable heterogeneous promoters that could overcome these difficulties.<sup>18,19</sup> The development of highly efficient Sn- and Zr-substituted zeolites with isolated Lewis acid centers has given a decisive impetus to CTH technology, as they are still among the most attractive catalysts for MPV reactions today. Studying their catalytic performances, it becomes clear that the partially hydrolyzed oxide surfaces,<sup>20,21</sup> which are consequently enriched with hydroxyl sites, are considered as active centers in these systems. Well-isolated active sites outperform those that are interconnected, and both the accessibility (e.g., open Sn sites) of the active sites<sup>20,22</sup> and the hydrophobicity of the active surface have a remarkable influence on their catalytic performance.<sup>20</sup> The presence of the hydroxyl groups is particularly important since the formation of reactive alkoxides can only occur with the aid of these groups.<sup>20–22</sup> This phenomenon can be readily related to the fact that strong Lewis acid and base sites cannot coexist on the same catalyst when using these zeolitic-based catalysts.<sup>18,23</sup>

The lack of this ability of MPV catalysts has motivated studies to develop new strategies based on the concept of heterogeneous Frustrated Lewis Pairs (FLP) or FLP-like catalysis.<sup>24,25</sup> In contrast to the popularity of homogeneous FLP catalysis,<sup>24</sup> few studies have focused on developing its heterogeneous counterpart,<sup>24–26</sup> and this concept is strongly limited to the application of CeO<sub>2</sub>-derived catalysts.<sup>25–28</sup> Remarkably, the first results obtained in the context of solid FLP-catalyzed CTH have demonstrated that an active, selective, and robust CeO<sub>2</sub>-based catalyst enabled the conversion of various carbonyl compounds, albeit under harsh reaction conditions (>alcohol excess of 100-fold,  $T = 160\text{ }^{\circ}\text{C}$ , high autogenous pressure,  $t = 24\text{ h}$ ).<sup>27,28</sup> To further improve the catalytic performance of CeO<sub>2</sub>, there are some significant challenges that are difficult to overcome. Particularly, both the generation of the defect sites and hydroxyl groups, the correct spatial distances between the active sites, and the stability of the active surface under the reaction conditions are not yet properly ensured, especially in a reproducible manner.<sup>25,28</sup> Furthermore, by increasing the Ce(III)/Ce(IV)-ratio of a ceria surface to facilitate MPV reactions, the surface charge ( $\xi$ -potential) of the solid

decreases and probably makes the adsorption of fully or partially negatively charged alcohols (alcoholates) more difficult, similar to the effect described for the nanozymatic applications of ceria.<sup>29</sup>

Given the results based on Zr/Sn-modified zeolite catalysts, it is hypothesized that isolated, well-established Ce(III)–O(H) centers inserted into a properly chosen host structure promote MPV reactions and outperform ceria. For this purpose, the use of nonactivated hydrotalcite [Mg<sub>3</sub>Al layered double hydroxide [named as layered double hydroxides (LDH)]] as a host structure would be a good option. LDH is built on brucite (Mg(OH)<sub>2</sub>)-like hydroxyl layers in which part of the Mg(II) centers are isomorphically substituted by trivalent cations [e.g., Al(III), Ga(III), Fe(III), and Ce(III)].<sup>30,31</sup> Due to this substitution, the hydroxyl layers have positive charges, which are balanced by the interlamellar anions (e.g., OH<sup>−</sup>, CO<sub>3</sub><sup>2−</sup> etc.).<sup>32–34</sup> With the cosubstitution of cerium cations in this structure [in addition to aluminum(III) centers], the stabilization of the Ce(III) oxidation state is expected to be similar to other valence-variable cations,<sup>35,36</sup> and the adequate isolation of the active sites associated with the required hydroxyl groups is possible based on the even cation distribution model. Furthermore, LDH has constant positive surface charge ( $\sim +30$  to  $40\text{ mV}$ ), which is highly independent from the guest cations cosubstituted in a small extent.<sup>32,37</sup> It is noteworthy that many studies have attempted to synthesize Ce-containing LDH.<sup>38,39</sup> However, to the best of our knowledge, it has not been possible to produce a phase-pure LDH structure when more than 1% cerium compared to the aluminum centers is used. This must be related to the relatively high ionic radius of cerium compared to Mg/Al cations, which makes substitution less favorable.<sup>40</sup> Fortunately in our group, there is a well-established procedure to insert high ionic radius cations [e.g. Gd(III)]<sup>41</sup> into the LDH structure, also in a procedure that protects lower oxidation states of the cations from oxidation.<sup>35,36</sup>

In this paper, a useful optimized strategy to produce Ce-containing, phase-pure LDH is shown. We present that selective MPV reductions can be enabled under ambient conditions by well-isolated Ce(III) active specimens inserted into LDH structures, and these active centers overperform the catalytic ability of inserted Ce(IV) specimens. The crucial role of both the surface hydroxyl groups and the structural distortion/defect sites in the LDH structure generated by the isomorphous substitution are elucidated. A clear relationship between the acid/base property of the modified LDH structures and their catalytic performances is also depicted.

## EXPERIMENTAL PART

**Materials.** All the chemicals were of reagent grade and were purchased from Merck or Sigma-Aldrich; they were used without further purification.

**Preparation of Hydrotalcites.** Ce-containing magnesium–aluminum LDH (hydrotalcites, LDHs) were synthesized by a simple coprecipitation method (named in the text as one-step procedure). MgCl<sub>2</sub> × 6H<sub>2</sub>O (3 mmol), (1 −  $x$ ) mmol AlCl<sub>3</sub> × 6H<sub>2</sub>O, and  $x$  mmol CeCl<sub>3</sub> × 7H<sub>2</sub>O ( $x = 0.01$ – $0.15$  mmol) were first dissolved in 15 mL water. This mother liquor was then quickly added to 20 mL of freshly prepared NaOH solution of 0.40 M under a N<sub>2</sub> atmosphere. After vigorous stirring for 45 min, the slurry obtained was centrifuged (4750 rpm for 5 min), washed twice with water and dispersed again (in 20 mL of water), and centrifuged (4750 rpm at 4 °C for 15 min after the first step and for 30 min after the second step). The prepared gel-like product was then thoroughly redispersed in 30 mL of water

and stored at room temperature for 3 days. Thereafter, the solidified final product was separated by centrifugation (4750 rpm at 4 °C for 15 min) and then dried at 75 °C in vacuo for 16 h. The LDHs obtained are labeled as MgAlCe<sub>x</sub>, where *x* is the initial Ce(III)/Al(III) molar ratio: MgAlCe<sub>0.01</sub>/MgAlCe<sub>0.15</sub>. Pure hydrotalcite (Mg<sub>3</sub>Al-LDH; denoted as MgAl) was prepared in the same method in the absence of cerium salt, using 10 mL of mother liquor and 20 mL of 0.4 M NaOH solution.

The one-step method described above was used to synthesize phase-pure products, but the method was severely limited in terms of the number of cerium centers. To overcome this limitation, a second two-step preparation method was introduced. In this method, exactly the same reaction steps as described above were repeated, until the final suspension was obtained. In this case, before the final step (separation/drying), the entire batch of cerium-containing slurry suspended in water (30 mL) was placed in a Teflon-lined stainless-steel autoclave with a capacity of 50 mL and then heat-treated at 110 °C for 16 h, followed by the final separation procedure. This method allowed the incorporation of cerium in a slightly extended concentration range [up to a cerium content of 15% compared to that of the Al(III) centers].

**Characterization Methods.** Powder X-ray diffraction (XRD) patterns of the solids were recorded on a Bruker D8 Advance powder XRD instrument by applying Cu K $\alpha$  radiation ( $\lambda = 0.15418$  nm) and 40 kV accelerating voltage at 40 mA in the range of  $2\theta = 5$ – $80^\circ$ . Dynamic light scattering (DLS) was used to measure the hydrodynamic size of the dispersed particles. The measurements were carried out with the same Nanosizer (Malvern) device as above at a  $175^\circ$  scattering angle in disposable plastic cuvettes.

The instrument for taking the Fourier-transform infrared (FT-IR) spectra was a Nicolet 5700 FT-IR spectrometer (Thermo Electron Corporation) with a  $2\text{ cm}^{-1}$  resolution in attenuated total reflection mode (ATR-FT-IR). Raman spectra were recorded with a portable IM-52 Raman Microscope (Snowy Range Instruments). The 785 nm laser wavelength with a laser power of 70 mW was used for excitation of Raman scattering. The first coordination sphere and oxidation state of the transition metal ions was established by using an X-ray photoelectron (XP) spectroscopic mapping. XP spectra (XPS) were recorded with a SPECS instrument equipped with a Kratos Axis Supra Plus XPS, under a main-chamber pressure in the  $10^{-9}$  to  $10^{-10}$  mbar range.

Nitrogen sorption isotherms of samples were obtained using a Quantachrome Autosorb-1 analyzer at 77 K. The [Brunauer–Emmett–Teller (BET)] specific surface areas were calculated using adsorption data at a relative pressure range of  $p/p_0 = 0.05$ – $0.25$ . The morphologies of the samples prepared were studied by scanning electron microscopy (SEM). The SEM images were recorded on an FEI Quanta 650 FEG at an acceleration voltage of 20.0 kV. The thermal behavior of the as-prepared layered composites was studied on a thermogravimetric analysis/differential scanning calorimetry 1 STARe System (Mettler-Toledo Ltd., AU).

The amount of Ce, Mg, and Al components in the nanoparticles was determined by inductively coupled plasma-atomic emission spectrometry (ICP-AES) using a Varian Vista Pro instrument. Ce(III) content and Ce(III)/Ce(IV) actual molar ratios were determined by fluorescence spectroscopy (FLS) measurements using a SHIMADZU RF-5301PC spectrometer with excitation and emission slits of 5 nm. The measurements were carried out at room temperature using  $\lambda_{\text{ex}} = 255$  nm and  $\lambda_{\text{em}} = 355$  nm.

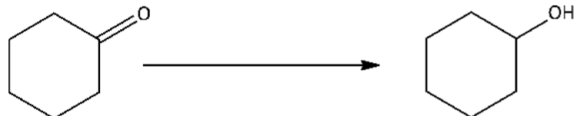
**Cyclohexanone Transfer Hydrogenation to Cyclohexanol in 2-PrOH.** The MPV reactions of cyclohexanone, which were used as test reactions to describe the catalytic performance of the as-prepared solids, were carried out in a batch reactor at a constant reaction temperature of 65 °C under a N<sub>2</sub> atmosphere. A solution of cyclohexanone ( $c = 0.5$  M) and the appropriate amount of 2-PrOH (2–4 mL) was stirred under the above-mentioned reaction conditions in the presence of a chosen hydrotalcite derivative (50–200 mg) for an appropriate reaction time (1–360 min). When the reaction was completed, the obtained slurry was cooled down to room temperature and then centrifuged at 10,000 rpm for 10 min to remove the catalyst.

The obtained mixture was then evaporated under reduced pressure and redissolved in 2-PrOH. Cyclohexanone conversions were determined by ultraviolet–visible (UV–vis) spectrophotometry in 2-PrOH on using the absorption band maximum of the cyclohexanone in the UV region ( $\lambda_{\text{max}} = 282$  nm). The UV–vis absorbances were detected on a SHIMADZU UV-2450 spectrophotometer. For determining the cyclohexanol yields, <sup>1</sup>H NMR measurements were introduced (Figure S1B,C). <sup>1</sup>H NMR spectra were recorded at room temperature on a Bruker AV-500 in DMSO-*d*<sub>6</sub>.

## RESULTS AND DISCUSSION

**Proof of Concept.** In order to confirm the underlying hypothesis, initial transfer hydrogenation of cyclohexanone as the model reaction (Figure S1 and Scheme S1) was investigated in the presence of the as-prepared, phase-pure MgAlCe<sub>0.05</sub>-LDH, which was chosen arbitrarily at this point. To put its catalytic performance into the right context, the obtained data were compared with other benchmark catalysts and building blocks of the composites (Table 1).

**Table 1.** MPV Reduction of Cyclohexanone Catalyzed by As-prepared Ce-Containing LDH and Benchmark Catalysts<sup>a</sup>



		cyclohexanone conversion (mol %) <sup>b</sup>	selectivity (mol %) <sup>c</sup>	cyclohexanol yield (mol %) <sup>d</sup>
1		<1		
2	MgAlCe <sub>0.05</sub> -LDH <sup>e</sup>	10 ± 1	100	10 ± 0.9
3	MgAl-LDH <sup>e</sup>	<1		
4	Cal. MgAl-LDH <sup>f</sup>	13 ± 0.8	100	13 ± 1.0
5	Reh. MgAl-LDH <sup>g</sup>	11 ± 0.7	100	11 ± 0.5
6	CeO <sub>2</sub>	4 ± 1	83	3 ± 0.4
7	NP CeO <sub>2</sub> <sup>h</sup>	7 ± 1	98	7 ± 0.7
8	ZrO <sub>2</sub>	35 ± 2	99	35 ± 0.9
9	Hyd. ZrO <sub>2</sub> <sup>i</sup>	45 ± 1	99	45 ± 1.4
10	MgO	6 ± 0.5	100	6 ± 0.4

<sup>a</sup>(Reaction conditions:  $c(\text{cyclohexanone}) = 0.5$  M;  $V(2\text{-propanol}) = 4$  mL;  $m(\text{catalyst}) = 100$  mg;  $T = 65$  °C;  $t = 5$  h under N<sub>2</sub> atmosphere.).

<sup>b</sup>Determined by UV–vis spectroscopy ( $n \rightarrow \pi^*$ ;  $\lambda = 270$  nm).

<sup>c</sup>Calculated: [(yield/conversion) × 100%]. <sup>d</sup>Determined by NMR spectroscopy.

<sup>e</sup>Modified coprecipitation (detailed recipe can be seen in Supporting Information). <sup>f</sup>Calcined ( $T = 500$  °C). <sup>g</sup>Calcined-hydrated. <sup>h</sup>CeO<sub>2</sub> nanoparticles. <sup>i</sup>Hydrated ZrO<sub>2</sub>.

As determined, no reaction occurred in the absence of any catalysts under the set reaction conditions. It is noteworthy that more or less standard conditions were chosen for this comparison but the reaction temperature applied ( $T = 65$  °C) was different from the standard one ( $T \geq 82$  °C).<sup>42</sup> Apart from the green chemistry point of view, the LDH host probably has a capability of promoting the self-condensation of cyclohexanone, which is favored at higher temperatures.<sup>43</sup>

As can be seen in rows 3–7, nonmodified, nonactivated LDH and CeO<sub>2</sub> did not have any notable activity to catalyze this reaction.<sup>44</sup> As expected, at this reaction temperature, CeO<sub>2</sub>-based catalysts were not highly active, while the inactivity of LDH can be readily associated with the lack of the appropriate amount of accessible Lewis acid centers on their surface.<sup>27,28</sup> After performing the activation procedure of

LDH, the obtained mixed oxides exhibited moderate activity with exclusive selectivity exceeding the performance of a pure MgO catalyst.<sup>45</sup> The tested ZrO<sub>2</sub>-type solids appeared to be highly active and selective (35–45 mol % cyclohexanol yield),<sup>46</sup> with the performance depending on the pretreatment of the catalyst, which is in good agreement with the literature data.<sup>22</sup> Upon using cerium-modified LDH as a promoter (Row 2), a moderate cyclohexanol yield of ~10% with remarkable selectivity was achieved. This performance surpassed the capability of both nonactivated LDH and CeO<sub>2</sub> as well as MgO and was close to the efficiency of the LDH-derived mixed oxides. As confirmed by the test reactions, the presented concept of interplay between isolated cerium centers and nonactivated LDH or activated LDH as the host is a viable alternative to useful MPV catalysts.

**Characteristics of As-prepared Ce-LDHs.** By using the well-established protocol developed previously in our group (one-step procedure), cosubstituted—in this case cerium-modified LDHs—phase-pure, highly crystalline solid samples were prepared [marked as MgAlCe<sub>x</sub>,  $x = n(\text{Ce})/(n(\text{Al}) + n(\text{Ce}))$ ]. The characteristic XRD patterns of these solids closely resemble that of phase-pure LDHs with the rhombohedral structure, which can be assigned into the layered double hydroxide of the 3R<sub>1</sub> polytype (Figure 1A; JCPDS card no. 89-

0460). In contrast, as compared to the characteristic reflections of nonmodified LDH (labeled as MgAl) synthesized in the same method, a significant shift into lower  $2\theta$  region of the XRD patterns of the solid products was observed, indicating the increase in the interlayer distance (Figure 1B). Thus, this change can be identified as an increase in the hydroxide layer thickness as a result of the larger cerium incorporation.<sup>47</sup> Moreover, the magnitude of this shift appeared to be proportional to the cerium content in the composites, confirming our assumption.

It is worth noting that cerium cations cannot be incorporated into MgAl in arbitrary amounts. There is a maximum initial cerium ratio of 10% to the total number of M(III) cations. Above this initial concentration, CeO<sub>2</sub> (JCPDS no. 34-0394) was formed as the second phase in all cases (Figure S2). This Ce amount range was extended to a maximum of 15% when a coprecipitation was performed and followed by hydrothermal treatment (two-step procedure). The use of values above this extended range is practically accompanied by the presence of ceria as a byproduct without any exception.

To confirm the cerium insertion and determine the actual molar ratio of Ce-to-(Al + Ce), the ICP-AES measurement was applied. As seen in Table 2, each modified sample contained cerium in a different amount and the actual ratios were indeed close to the initial ones (incorporation rate = 95–98%) when the one-step procedure was used. However, a slightly larger difference was observed for the maximum initial concentration of cerium (90%). Those rates were significantly lower (75–81%) for the products prepared using the two-step procedure. It should also be mentioned that the actual Mg/M(III) ratio was almost identical to the theoretical one (3:1) in all cases. Furthermore, the TG/DTG analysis of the products showed that there were no remarkable changes in the actual composition of the LDHs compared to one another and to their nonmodified counterpart (Figure S3). Taking into account the results of the analytical methods presented, the most probable composition of the LDHs was calculated, as listed in Table 2. In addition, BET measurements confirmed that the specific surface area of the original MgAl structure did

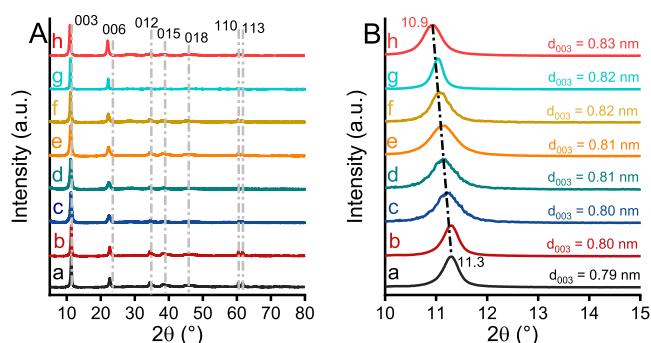


**Figure 1.** XRD patterns of the as-prepared (a) MgAl, (b) MgAlCe<sub>0.01</sub>, (c) MgAlCe<sub>0.025</sub>, (d) MgAlCe<sub>0.05</sub>, (e) MgAlCe<sub>0.075</sub>, (f) MgAlCe<sub>0.1</sub>, (g) MgAlCe<sub>0.125</sub>, and (h) MgAlCe<sub>0.15</sub> in the  $2\theta$  range of (A) 5–80° and (B) 10–15° (MgAlCe<sub>0.125</sub> and MgAlCe<sub>0.15</sub> were synthesized via a two-step procedure, see Supporting Information).

**Table 2.** Actual Ce/Al and Mg/M(III) Molar Ratios, Interlamellar Water Content, and Calculated Compositions of the As-prepared LDHs

LDH composite <sup>a</sup>	Ce/(Al + Ce) ratio (%) <sup>b</sup>	Mg/M(III) ratio <sup>c</sup>	specific surface area (m <sup>2</sup> /g) <sup>d</sup>	interlamellar water ratio (m/m %) <sup>e</sup>	incorporation rate (%) <sup>e</sup>	composition <sup>f</sup>
MgAl	—	2.98	81	11	—	Mg <sub>2.98</sub> Al(OH) <sub>7.96</sub> (CO <sub>3</sub> ) <sub>0.5</sub> × 2.1 H <sub>2</sub> O
MgAlCe <sub>0.01</sub>	0.95	2.99	60	11	95	Mg <sub>2.99</sub> Al <sub>0.9905</sub> Ce <sub>0.0095</sub> (OH) <sub>7.98</sub> (CO <sub>3</sub> ) <sub>0.5</sub> × 1.9 H <sub>2</sub> O
MgAlCe <sub>0.025</sub>	2.43	2.97	85	11	97	Mg <sub>2.97</sub> Al <sub>0.9757</sub> Ce <sub>0.0243</sub> (OH) <sub>7.94</sub> (CO <sub>3</sub> ) <sub>0.5</sub> × 2.5 H <sub>2</sub> O
MgAlCe <sub>0.05</sub>	4.82	2.98	73	11	96	Mg <sub>2.98</sub> Al <sub>0.9518</sub> Ce <sub>0.0482</sub> (OH) <sub>7.96</sub> (CO <sub>3</sub> ) <sub>0.5</sub> × 2.5 H <sub>2</sub> O
MgAlCe <sub>0.075</sub>	7.13	2.97	71	11	95	Mg <sub>2.97</sub> Al <sub>0.9287</sub> Ce <sub>0.0713</sub> (OH) <sub>7.94</sub> (CO <sub>3</sub> ) <sub>0.5</sub> × 2.4 H <sub>2</sub> O
MgAlCe <sub>0.1</sub>	9.03	2.96	80	11	90	Mg <sub>2.96</sub> Al <sub>0.9097</sub> Ce <sub>0.0903</sub> (OH) <sub>7.92</sub> (CO <sub>3</sub> ) <sub>0.5</sub> × 2.4 H <sub>2</sub> O
MgAlCe <sub>0.125</sub>	10.10	2.95	84	11	81	Mg <sub>2.95</sub> Al <sub>0.8990</sub> Ce <sub>0.1010</sub> (OH) <sub>7.90</sub> (CO <sub>3</sub> ) <sub>0.5</sub> × 2.4 H <sub>2</sub> O
MgAlCe <sub>0.15</sub>	11.25	2.95	69	11	75	Mg <sub>2.95</sub> Al <sub>0.8875</sub> Ce <sub>0.1125</sub> (OH) <sub>7.90</sub> (CO <sub>3</sub> ) <sub>0.5</sub> × 2.3 H <sub>2</sub> O

<sup>a</sup>Ce<sub>x</sub> ( $X = n(\text{Ce})/n(\text{Al}) \times 100\%$ ). <sup>b</sup>Determined by ICP-AES. <sup>c</sup>Determined by TG/DTG. <sup>d</sup>Determined by BET measurements. <sup>e</sup>Success rate =  $(n(\text{Ce})_{\text{initial}}/n(\text{Ce})_{\text{actual}}) \times 100\%$ . <sup>f</sup>Calculation based on ICP-AES and TG/DTG results.

not vary significantly as a result of cerium insertion (Table 2, Figure S5).

Moreover, the ATR-FT-IR spectra (Figure 2) provide evidence for the presence of the carbonate as charge

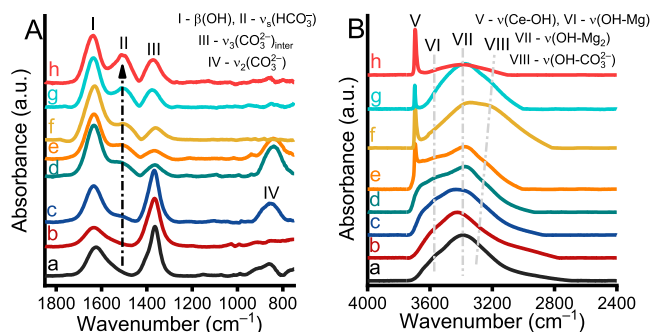


**Figure 2.** ATR-FT-IR spectra of (a) MgAl, (b) MgAlCe<sub>0.01</sub>, (c) MgAlCe<sub>0.025</sub>, (d) MgAlCe<sub>0.05</sub>, (e) MgAlCe<sub>0.075</sub>, (f) MgAlCe<sub>0.1</sub>, (g) MgAlCe<sub>0.125</sub>, and (h) MgAlCe<sub>0.15</sub> in the wavenumber range of (A) 1850–800 and (B) 4000–2400 cm<sup>-1</sup>.

compensating anions, represented by characteristic absorption bands at 1363 ( $\nu_3$  CO<sub>3</sub><sup>2-</sup>); peak III and 863 cm<sup>-1</sup> ( $\nu_2$  CO<sub>3</sub><sup>2-</sup>), peak IV.<sup>33</sup> However, considering our previous findings,<sup>33</sup> it could be excluded that a significant amount of surface adsorbed carbonate would be enriched, which has a readily identifiable characteristic band around 1405–1410 cm<sup>-1</sup> (Figure S4). This fact is of great importance because nonactivated LDHs often show lower catalytic activity due to the presence of counterions on the surface that mask the active (hydroxyl) sites.<sup>48</sup> Besides, IR spectra include well-known, overlapped absorption band of water molecules and hydroxyl functions (peaks I, V–VIII).<sup>33</sup> It can be seen that in the high wavenumber region (Figure 2B), both the peak positions and the intensities for various O–H bonds changed significantly when increasing the cerium content, which underpins the fact of the isomorphous cosubstitution.<sup>49</sup>

More interestingly, a new vibration band around 1510 cm<sup>-1</sup> came in the spectra of cerium-containing LDHs (Figure 2A; peak II), which is increasing in intensity with increasing cerium-content. It is difficult to identify this band beyond doubt, but probably it can be associated with the stretching mode vibrations of bicarbonate or bidentate carbonate specimens bound to the surface.<sup>50</sup> Obviously, the occurrence of bicarbonate or bidentate carbonate specimens is not possible without the coexistence of Ce(IV)/defect centers.<sup>50</sup> This can be illustrated using the analogies described for Ti<sup>4+</sup> centers in TiO<sub>2</sub> (Scheme 1).<sup>51</sup> Nonetheless, it is difficult to state whether these Ce(IV)-containing specimens are inserted into the lattice or whether noncrystalline/smaller-sized CeO<sub>2</sub> is formed to a lesser extent.

**Structural Features of the Ce-Insertion into an LDH Lattice.** To prove the coexistence of Ce(III)/Ce(IV) centers

and determine their actual molar ratio in the as-prepared LDHs, fluorescence spectroscopic (FLS) measurements were introduced in such a way that LDHs were dissolved in nonoxidative acid (Figure 3). The use of this method is based

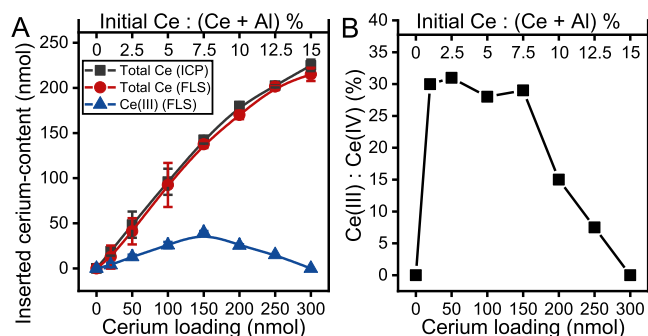


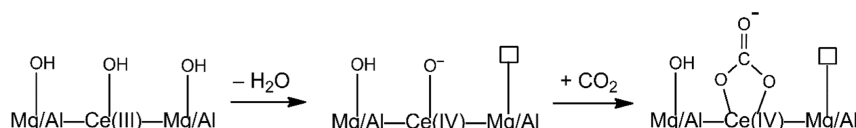
**Figure 3.** (A) Inset total cerium-content and Ce(III)-content in the as-prepared LDHs (measured by ICP-AES and FLS) as a function of the initial cerium loading as well as (B) Ce(III)-to-Ce(IV) actual molar ratios in the as-prepared samples calculated from FLS results as a function of the initial cerium loading.

on the fact that Ce(III) specimens exhibit fluorescence in contrast to Ce(IV) species.<sup>52</sup> As shown in Figure 3A, the determined total cerium concentrations, which was measured after the complete reduction of Ce(IV) ions with sodium sulfite,<sup>53</sup> appeared to be in good agreement with the data measured by ICP-AES. The growth of the inserted total cerium amount was monotonic as a function of the initial cerium concentration (Figure 3A), regardless of the synthesis method used.

Otherwise, the cerium(III) concentration was found to change as a reverse “V” curve in relation to the initial cerium concentration, which had a maximum value at  $x = 7.5\%$ . Furthermore, no detectable cerium(III) content was observed when this ratio of nominal replacement reached 15%, but there were more Ce(IV) specimens than Ce(III) in the samples (Figure 3B). In analogy to the insertion of Sn(IV) cations into LDH hosts, it is theoretically possible that these Ce(IV) centers are incorporated into the LDH lattice by isomorphous (co)substitution.

XPS measurements were performed to determine the Ce(III)/Ce(IV) ratio on the active surfaces (Figure 4A,B; Figures S6 and S7; Table S4). The Ce<sub>3d</sub> binding energy (BE) range of almost all Ce-containing LDH samples was fully described by including six well-known fitting components of Ce<sup>4+</sup> specimens and four corresponding peaks of Ce<sup>3+</sup> specimens surrounded by oxygen atoms in the fitted model (Figure 4A, S6, Table S4).<sup>54</sup> It should be noted here that the MgAlCe<sub>0.01</sub> sample was excluded from this XPS analysis, which had too low levels of cerium cations on the surface to allow the precise interpretation of the data. As for MgAlCe<sub>0.125</sub> and

**Scheme 1. Plausible Mechanism of the Formation of Surface Defect Sites and Surface Adsorbed Bidentate Carbonate Species (Bicarbonate May Form via the Hydration of Bidentate Carbonate Specimen; Surface Defect Sites are Marked with Small Square)**



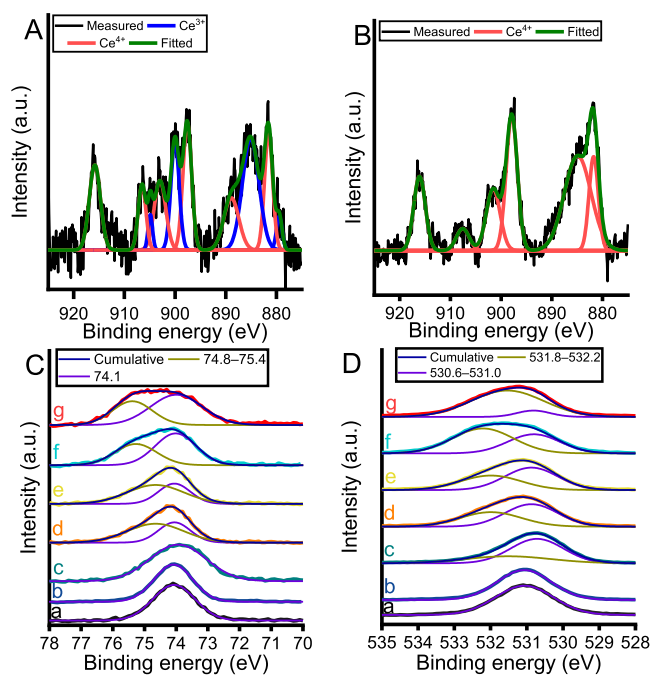


**Figure 4.** XP spectra of the Ce-containing LDHs.  $Ce_{3d}$  XP spectra of (A)  $MgAlCe_{0.075}$  and (B)  $MgAlCe_{0.15}$ . (C)  $Al_{2p}$  and (D)  $O_{1s}$  XP spectra of (a)  $MgAl$ , (b)  $MgAlCe_{0.025}$ , (c)  $MgAlCe_{0.05}$ , (d)  $MgAlCe_{0.075}$ , (e)  $MgAlCe_{0.1}$ , (f)  $MgAlCe_{0.125}$ , and (g)  $MgAlCe_{0.15}$ .

$MgAlCe_{0.15}$ , the corresponding curves were fitted by considering only the peaks of the  $Ce^{4+}$  specimens (Figures 4B and S6). The change in the determined Ce(III)/Ce(IV) ratio (Figure S7) showed a good correlation with the trend ascertained by FLS.

Interestingly, the chemical environment of both the aluminum and oxygen atoms differs from that in pure LDH due to the isomorphous substitution. The  $Al_{2p}$  region of  $MgAl$  was readily described by only one parameter associated with the Al–O BE (74.1 eV) of the octahedrally coordinated, hydrated alumina lattice specimen in the  $MgAl$ -LDH (Figure 4C).<sup>55</sup> On the contrary, at a nominal cerium loading higher than 5%, a second aluminum environment (BE of 74.8–76.4 eV) must be included in the model. This second environment strongly resembles that of tetrahedrally coordinated, partially hydrated alumina centers in  $MgAlCe$ -LDHs.<sup>56</sup> This has indirectly proved the insertion of Ce(III)/Ce(IV) centers into the lattice and shown that the existence of the aforementioned defect sites (Scheme 1) is established. Parallel to this trend, a second chemical environment of oxygen specimens was also formed in the lattice (Figure 4D). It should be noted here that the  $O_{1s}$  XPS measurements further support the assumption that hydroxyl groups (BE  $\sim$  532 eV) can be found on the surface while the presence of the carbonate specimens can be excluded.<sup>57</sup> This finding is further supported by the  $C_{1s}$  spectra of the LDHs (Figure S6).<sup>57</sup> As for the  $O_{1s}$  region, there was no evidence for the existence of oxygen atoms in a chemical environment similar to that of  $CeO_2$ .<sup>54</sup> Accordingly, all of the cerium spectra obtained belongs to inserted cerium centers.

To determine whether tetrahedrally coordinated aluminum centers are truly formed in LDHs, as suggested in the XPS studies,  $^{27}Al$ -solid-state (SS)-NMR spectra were recorded (Figure 5A). A significant broadening of the basic peak associated with octahedrally coordinated lattice aluminum

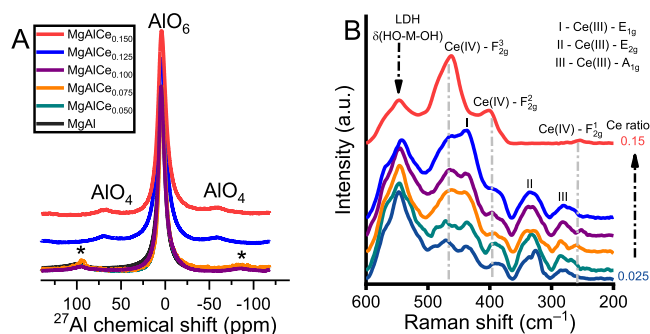


**Figure 5.** (A)  $^{27}Al$ -SS-NMR spectra and (B) Raman spectra of the as-prepared LDHs. (The color coding is the same in both graphs).

centers ( $\sim$ 4.38 ppm)<sup>58</sup> was observed in the presence of cerium cations loaded to an extent of 1–7.5% compared to the aluminum centers in  $MgAl$ ; otherwise there was no difference. Using a higher initial concentration of cerium, fingerprint-like chemical shifts around 70 ppm known to belong to the tetrahedrally coordinated aluminum centers appeared in the NMR spectra.<sup>58</sup> These are likely formed by the incorporation of Ce(III)/Ce(IV) cations into the lattice (Scheme 1). However, these partially hydrated alumina centers should be considered as defect sites since they coexist in a double hydroxide layer surrounding with octahedrally coordinated, fully hydrated magnesium/aluminum centers. Note that the XPS method is a surface sensitive method, whereas the SS-NMR method is bulk sensitive. Accordingly, the observed trends of the two methods differ slightly due to quantitative differences in this case.

However, the existence of the specimens described above does not exclude the formation of other types of defect sites that could be related to the Ce(III)/Ce(IV) interaction. This can be readily verified by Raman spectroscopy (Figures 5B and S8). As reported by Schilling et al. and Liu et al.,<sup>59,60</sup> Raman spectra allow us to distinguish the “real” oxygen vacancies near the  $Ce^{4+}$  centers (500  $cm^{-1}$ ), the  $Ce^{3+}$  centers (or other vacancies) in the second coordination sphere of the  $Ce^{4+}$  centers (470–480  $cm^{-1}$ ), and the  $CeO_2$ -like environment (455  $cm^{-1}$ ). In the Raman spectrum of pure LDH (Figure S8), there is only one broadened peak (545  $cm^{-1}$ ) in the range (600–200  $cm^{-1}$ ), which is due to a combination of bending mode vibrations of Al–OH and Mg–OH units [ $\delta(OH-M-OH)$ ].<sup>61</sup> For comparison, both a physically mixed composite of  $MgAl$ -LDH and  $CeO_2$  and LDH-supported  $CeO_2$  prepared by wet impregnation were synthesized. In their Raman spectra (Figure S8), beside the peak of the LDH structure that remained, a new peak appeared at 460  $cm^{-1}$ , attributed to the  $F_{2g}$  vibrational mode of fluorite-type  $CeO_2$ .<sup>59,60</sup> All of the measured Raman spectra of the Ce-LDHs were fitted into seven different Raman bands (Figure 5B). As expected, the fingerprint-like band of the LDH lattice was readily found at a slightly shifted band position of 550  $cm^{-1}$ . Three other bands at 473, 390, and 260  $cm^{-1}$  were associated with Ce(IV)-containing specimens, which are identified as  $F_{2g}(3)$ ,  $F_{2g}(2)$ , and  $F_{2g}(1)$  bands, respectively. Considering the red shift of the  $F_{2g}(3)$  band, it is assumed that the Ce(IV) centers do not bind directly to defect sites but Ce(III) cations (or other defect sites) occupy part of the lattice positions in their second coordination sphere. Obviously, cerium(III) cations were incorporated into a chemical environment in hydroxide layers almost identical to that in  $Ce(OH)_3/Ce(H_2O)_x^3-$ , as reflected

by three Raman peaks associated with the Raman bands  $A_{1g}$  ( $\sim 284\text{ cm}^{-1}$ ),  $E_{2g}$  ( $\sim 340\text{ cm}^{-1}$ ), and  $E_{1g}$  ( $433\text{ cm}^{-1}$ ) of the  $\text{Ce}(\text{OH})_3$ -like structure.<sup>62</sup> Compared to the reported data, there was a clear blue shift in the  $E_{1g}$  band, which probably means that these centers are integral parts of the hydroxide layers. In the case of  $\text{MgAlCe}_{0.15}$ , all three Raman bands of the  $\text{Ce}(\text{III})$  specimens disappeared, consistent with the fluorescence data that the  $\text{Ce}(\text{III})/\text{Ce}(\text{IV})$  ratio was close to zero.

#### Acid–Base Properties of the As-prepared Samples.

Since MPV reactions are acid–base catalyzed reactions, it is critical to investigate the effects of cerium insertion in relation to the basicity and acidity of the solid samples.<sup>63</sup> Thus, ATR-FTIR probing measurements were conducted using probe molecules, in particular pyridine<sup>64</sup> to characterize the acidic centers and methanol<sup>65</sup> to measure the basic centers.

As shown in Figure 6A, four different characteristic absorption bands were observed in the spectra of pyridine

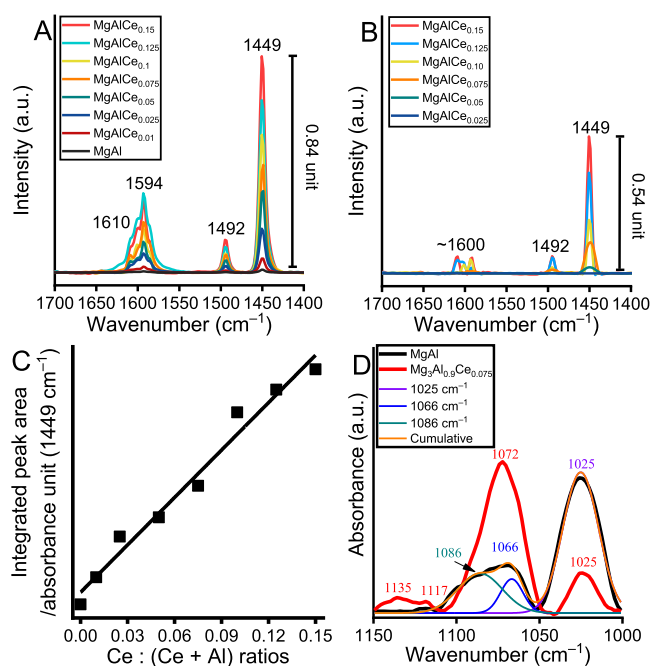


**Figure 6.** ATR-FT-IR spectra recorded after (A) adsorption of pyridine at room temperature on the samples and (B) adsorption of pyridine at room temperature on the samples followed by desorption at  $T = 125\text{ }^\circ\text{C}$ . (C) Integrated peak area of the peaks at  $1449\text{ cm}^{-1}$  as a function of initial Ce/Al ratios. (D) ATR-FT-IR spectra recorded after adsorption of methanol at room temperature on the samples. (All the presented spectra are difference spectra obtained after the subtraction of the corresponding spectra of the LDHs without adsorbed probe molecules.)

adsorbed on  $\text{MgAlCe}$  samples at  $1610$ ,  $1594$ ,  $1492$ , and  $1449\text{ cm}^{-1}$  in the fingerprint region ( $1700\text{--}1400\text{ cm}^{-1}$ ). According to the literature report of pyridine adsorption,<sup>64</sup> these bands are assigned to coordinatively bound pyridine ( $1449$  and  $1610\text{ cm}^{-1}$ ) adsorbed on Lewis acid centers and physisorbed pyridine ( $1594\text{ cm}^{-1}$ ). The absorption band at  $1492\text{ cm}^{-1}$  is a combination band containing vibrational components of both coordinately bound pyridine and pyridinium ions produced by the reaction of pyridine and Brønsted acids. However, the presence of Brønsted acid sites could be ruled out since bands around  $1638$  and  $1545\text{ cm}^{-1}$  were not observed at all. To confirm this assignment, the measurement

was repeated after desorption at a higher temperature ( $T = 125\text{ }^\circ\text{C}$ ; Figure 6B). As expected, the peak intensity of the strongly bound pyridine samples ( $1610$ ,  $1492$ , and  $1449\text{ cm}^{-1}$ ) decreased to varying degrees as a function of acid strength, while the peak associated with physisorbed pyridine decreased sharply in the intensity. It is noted that there were relatively large differences in the peak intensity of pure and Ce-modified LDHs, which were increased at higher outgassing temperatures. There were no peaks in the spectra of pure LDH and  $\text{MgAlCe}_{0.01}$  when a higher outgas temperature was used (not shown). As previously reported,<sup>66</sup> pure, nonactivated LDHs have very weak Lewis acidity due to hydration of the basic Brønsted centers. This Lewis acidity is considerably enhanced by Ce insertion, which explains the increased catalytic activity during transfer hydrogenation. Plotting the integrated peak areas of the characteristic band of  $1449\text{ cm}^{-1}$  as a function of the initial Ce:(Al + Ce) ratios in the LDHs revealed a linear trend (Figure 6C), indicating that both  $\text{Ce}(\text{III})$  and  $\text{Ce}(\text{IV})$  centers are accessible Lewis acid centers on the surface, and their active role will be reflected during the subsequent catalytic reactions.

Interestingly, cerium incorporation has also caused a slight change in basicity in LDHs (Figure 6D). Three characteristic adsorption bands were identified in the spectrum of the pure LDH at  $1086$ ,  $1066$ , and  $1025\text{ cm}^{-1}$  in the range  $1150\text{--}1000\text{ cm}^{-1}$ . These belong to the methoxy specimens of the bidentate linkage originating from the bond cleavage of the OH group of methanol ( $1086\text{ cm}^{-1}$ ; species II), undissociated methanol molecules adsorbed on Mg–OH units ( $1066\text{ cm}^{-1}$ ), and Al–OH units ( $1025\text{ cm}^{-1}$ ),<sup>65</sup> respectively. Looking at the spectra of cerium-modified structures, a similar envelope of spectra with three components at positions of  $1135\text{--}1117$ ,  $1072$ , and  $1025\text{ cm}^{-1}$  was observed (Figures 6D and S9). The last two components show adsorption of undissociated methanol. More interestingly, the absorption bands above  $1110\text{ cm}^{-1}$  can be attributed to dissociated methanol molecules, especially methoxy species with monodentate linkage (species I).<sup>65</sup> Considering the generally accepted mechanism of MPV reactions, species I is of particular importance in the activation of hydrogen sources (alcohol molecules). Accordingly, apart from the significantly more Lewis acid centers in cerium-modified LDHs compared to those in pure LDH, this aspect is certainly important with regard to the increased catalytic activity.

**Optimization of Conditions for Ce-LDH Catalyzed MPV Reduction of Cyclohexanone.** By introducing a Box–Behnken design<sup>67</sup> (BBD; Figure 7, Table S1) optimization procedure, the external reaction conditions [catalyst loading ( $50$ ,  $100$ , and  $200\text{ mg}$ ), hydrogen donor used (EtOH, 2-propanol and 2-butanol) and alcohol excess ( $1$ ,  $3$ , and  $5\text{ mL}$ )] were optimized when the cyclohexanone concentration ( $c = 0.5\text{ M}$ ), the reaction temperature ( $T = 65\text{ }^\circ\text{C}$ ), and the reaction time ( $t = 5\text{ h}$ ) were fixed under an  $\text{N}_2$  atmosphere.

Clearly, the use of  $\text{MgAlCe}_{0.05}$  with a loading of  $100\text{ mg}$  and an isopropanol volume of  $3\text{ mL}$  maximized the cyclohexanone yield. Moreover, both ethanol and 2-butanol could serve as the hydrogen donor in this MPV reaction, but the use of 2-propanol significantly increased the yield. These BBD tests also confirmed that the catalyst efficiency started to decrease immediately under an oxidative atmosphere, indicating the necessity of a  $\text{N}_2$  atmosphere during the catalytic reaction, probably related to the oxidizable feature of  $\text{Ce}(\text{III})$  centers (Figure S10) since characteristic reflections of  $\text{CeO}_2$  appeared

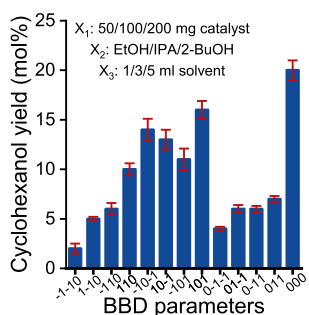


**Figure 7.** Experimental runs of the BBD. [Parameter web:  $X_1$ : -1 = 50 mg catalyst ( $\text{MgAlCe}_{0.05}$ ); 0 = 100 mg catalyst; 1 = 200 mg catalyst;  $X_2$ : -1 = EtOH (used as H-source and solvent); 0 = 2-propanol; 1 = 2-butanol;  $X_3$ : -1 = 1 mL solvent; 0 = 3 mL; 1 = 5 mL].

in the XRD patterns of this LDH after the reactions (Figure S11). Under the optimized reaction conditions, a 20% cyclohexanol yield with 100% selectivity was achieved in the presence of  $\text{MgAlCe}_{0.05}$  as the catalyst. When this reaction was repeated in air, the cyclohexanol yield was reduced to 3%.

**Structure–Activity Relationship.** With the optimized reaction conditions in hand, we examined the effects of the structural features of the Ce-containing LDH structures on their catalytic performance. Repeatedly note that as-prepared phase-pure LDHs had very similar specific surface area (Table 2), crystallite size, and morphology (Figure S5 and Table S3). As shown in Figure 8A, the reaction marker (cyclohexanol yield) changed with increasing amounts of incorporated cerium in the LDH layers. The trend can be described with an asymmetric volcano-like curve, which has a maximum yield at a cerium ratio of 7.5% to the amount of total M(III) centers. In the first regime, the gradual increase of cerium centers inserted into LDH leads to improved activity. Accordingly, this regime was fitted into an almost perfectly linear trend line. Clearly in the second regime, the increase of the nominal Ce concentration over 7.5% decreased the yield. Following this observation, it seems a plausible explanation that the catalytic activity decreases in parallel with the decrease in the number of Ce(III) centers on the surface in this regime in a linear trend. However, this does not lead to a complete loss of catalytic activity, since the Ce(IV) centers also exhibit some catalytic activity for MPV reactions at a much lower level than Ce(III) centers.<sup>68</sup> Same correlation between the activity of Ce(III) and Ce(IV) centers, in terms of transfer hydrogenation reactions, has already been observed in the homogeneous phase.<sup>68</sup>

Nevertheless, the catalytic performance of the optimized catalyst ( $\text{MgAlCe}_{0.075}$ ) does not fit into any of the two linear trends. It is assumed that in this Ce-LDH, predominantly Ce(III) centers should be considered as active sites, and aluminum-based defect sites already coexist on the surface of the catalyst to facilitate the catalytic performance. In this case, the interplay between Ce(III)/Ce(IV) and defect sites might be considered as FLP-like behavior. To support this assumption, the kinetic curves of the MPV reactions catalyzed by three different Ce-LDH catalysts were recorded (Figure 8B). The three catalysts were selected from three different regimes of the presented activity trend. All kinetic curves exhibit a well-formed sigmoidal growth trend, likely due to a pseudo second order kinetics. The first regime of these curves is linear enough to determine TOF values (Figure 8C). Considering all cerium centers as possibly active centers, the

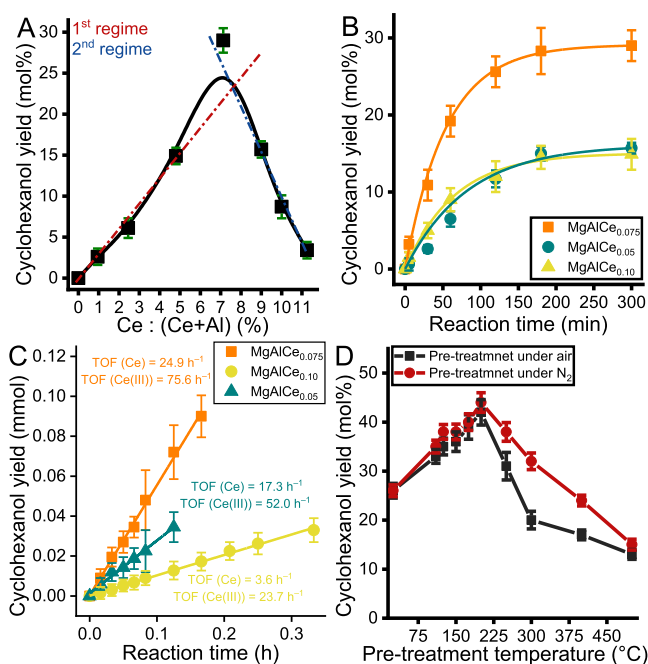


**Figure 8.** (A) Impact of the concentration of the inserted cerium centers on their own catalytic performance of the as-prepared LDHs toward transfer hydrogenation of cyclohexanone to cyclohexanol under the optimized reaction conditions [ $c(\text{cyclohexanone}) = 0.5 \text{ M}$ ;  $V(2\text{-propanol}) = 3 \text{ mL}$ ;  $m(\text{catalyst}) = 100 \text{ mg}$ ;  $T = 65 \text{ }^\circ\text{C}$ ; under a  $\text{N}_2$  atmosphere] in 5 h. (B) Kinetic profile of the cyclohexanone-to-cyclohexanol reaction catalyzed by three different Ce-containing LDHs under the optimized reaction conditions. (C) Determination of TOF values of the chosen LDHs through cyclohexanone-to-cyclohexanol transformations under the optimized reaction conditions. (D) Impact of the (pre)heat treatment of the chosen catalyst ( $\text{MgAlCe}_{0.075}$ ) on its own catalytic performance in CTH of cyclohexanone-to-cyclohexanol reactions under the optimized reaction conditions in 3 h.

TOF values differ significantly. Repeating the calculation was repeated by considering only Ce(III) centers as active centers; almost the same differences were obtained. Different TOF values must be associated with the different number and activity of active centers.<sup>18</sup> Thus, our assumption is partially proven because the accessibility of active centers, especially Ce(III) centers, may differ from each other in different samples depending on the Ce(III) number and the Ce(III)/Ce(IV) ratio. Nonetheless, this hypothesis can explain the fact that a cyclohexanol yield of 29% (25% within 2 h) was obtained via promoting the MPV reaction with  $\text{MgAlCe}_{0.075}$ , which is very close to the efficiency of the benchmark  $\text{ZrO}_2$  catalyst.

To underpin our hypothesis that the existence of the FLP-like specimens on the surface, a combined  $\text{O}_2$ -,  $\text{NH}_3$ -, and  $\text{CO}_2$ -T(emperature)P(rogrammed)D(esorption) study was initialized (Figure S12) focusing on the comparison of MgAl and  $\text{MgAlCe}_{0.075}$  samples.<sup>28</sup> Both  $\text{O}_2$ -TPD profiles consisted of two separately occurring desorption peaks in the relatively high temperature range of 380–650  $^\circ\text{C}$  (Figure S12A). These can be readily associated with the desorption of surface lattice oxygen (380–500  $^\circ\text{C}$ ), while the bulk lattice oxygen desorbed above 500  $^\circ\text{C}$ . For  $\text{MgAlCe}_{0.075}$ , a third desorption peak also appeared at 100–150  $^\circ\text{C}$  which is the desorption of surface chemisorbed oxygen specimens which are normally located at surface defect sites, particularly oxygen or hydroxyl vacancies. This indicates that hydroxyl vacancies exist on the surface of



the  $\text{MgAlCe}_{0.075}$  catalyst and can act as Lewis acid sites. Furthermore, unsaturated Lewis acid sites near these defect sites tend to form FLP structures with Lewis base sites. The presence of Lewis base sites can be readily detected by  $\text{CO}_2$ -TPD measurements (Figure S12B). As we can see, the  $\text{CO}_2$ -TPD profile of  $\text{MgAlCe}_{0.075}$  is very similar to that of  $\text{MgAl}$ , as it contains only one desorption peak in the temperature range of 200–250 °C, which is related to the weak basic sites, probably –OH groups with a Lewis base character. However, its maximum is shifted to higher temperatures (200 → 220 °C) compared to that of pure hydrotalcite, indicating the presence of stronger basic sites. There are two desorption peaks in the  $\text{NH}_3$ -TPD profile of  $\text{MgAlCe}_{0.075}$  at 180 and 310 °C (Figure S12C). Considering the lack of acidity of pure hydrotalcite (no desorption peak in its  $\text{NH}_3$ -TPD profile),<sup>69</sup> this is sufficient evidence that unsaturated Lewis acid centers can be found on the surface. If we add to this the proven coexistence of hydroxyl vacancies and slightly reinforced Lewis base centers, we are firmly convinced that FLP specimens form on the surface of the  $\text{MgAlCe}_{0.075}$  catalyst.

One of the main cornerstones of our hypothesis is that hydroxyl groups play an important role in catalytic performance. To demonstrate the correctness of this assumption, heat treatment of the catalyst at various temperatures in its initial state was performed (Figure 8D). As the observed changes were due to the conversion of Ce(III) → Ce(IV) on the surface, the pretreatment was carried out under a  $\text{N}_2$  atmosphere and air in each run for comparison. Based on the TG/XRD curves (Figures S3 and S13), the catalytic performance of the  $\text{MgAlCe}_{0.075}$  was expected to remain unchanged when the pretreatment temperature was changed until surface dehydroxylation occurred. Contrary to this assumption, pretreatment at 100 and 200 °C produced more active catalysts, with the cyclohexanol yield increasing to 33 and 42%, respectively (Figure 3). In this temperature range, two significant mass losses, i.e., the loss of adsorbed water (~111 °C) and interlamellar water (~200 to 270 °C), occurred. However, this dehydration did not cause the collapse of the long-range ordered layer structure of LDH. The observed increase in cyclohexanol yield is likely related to the exposure of active sites on the surface of the catalyst after the removal of these water molecules that associate with and block the OH active sites. At a pretreatment temperature above 250 °C, the structure of the modified LDHs gradually collapses, resulting from dihydroxylation of the active hydroxyl groups on the surface and leading to decreased yields. Moreover, a redistribution of the cation order probably also occurs at above 250 °C, as described in the literature on the thermal behavior of LDH.<sup>70</sup> As a result, the new active surface is enriched in MgO specimens; thus, the surface properties do not meet the requirements of FLP catalysis, and the efficiency of the formed bifunctional mixed oxide catalyst is far from that of its counterpart in the initial state. Accordingly, the studied catalyst is probably considered a solid FLP-like catalyst.

**Heterogeneity, Recyclability, and Versatility of  $\text{MgAlCe}_{0.075}$  Catalyst.** The heterogeneity of  $\text{MgAlCe}_{0.075}$  pretreated at 200 °C was demonstrated by a hot filtration test (Figure 9A) performed under the optimized reaction conditions. The actual catalyst was removed from the reaction mixture after 30 min, and the reaction was then continued with the filtrate for another 90 min. As shown in Figure 9A, the catalytic reaction was stopped by filtering out the Ce-LDH catalyst from the system, indicating that no active specimens

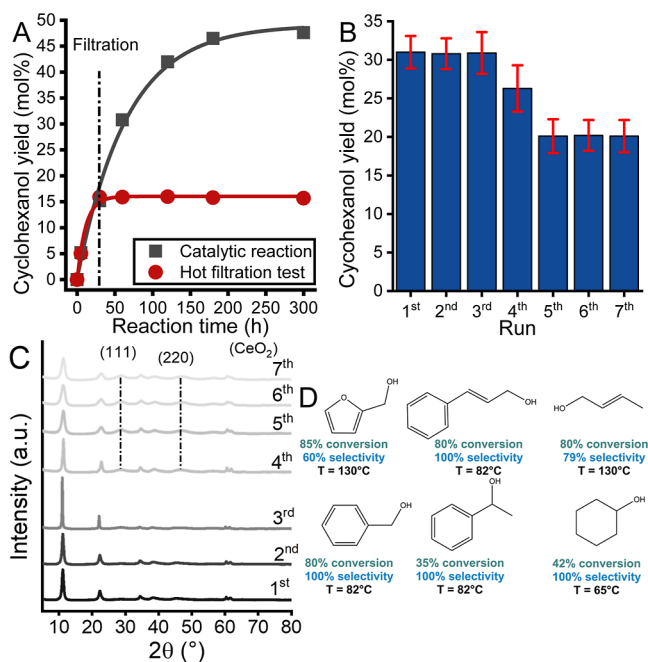


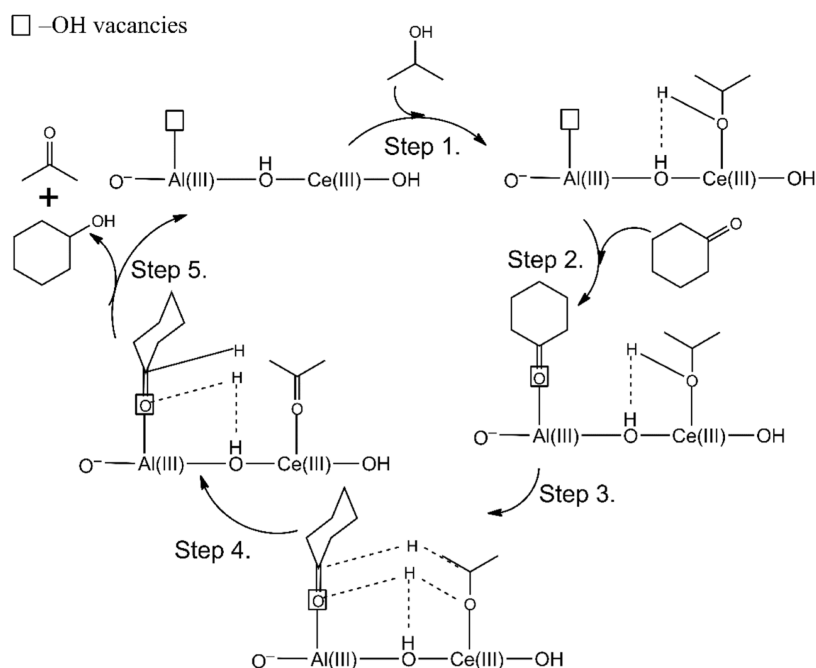
**Figure 9.** (A) Hot filtration and (B) recycling tests (reaction time: 1 h) of the heat treated (200 °C)  $\text{MgAlCe}_{0.075}$  solid in a cyclohexanone-to-cyclohexanol transfer hydrogenation. [Reaction parameters:  $c(\text{cyclohexanone}) = 0.5 \text{ M}$ ;  $V(2\text{-propanol}) = 3 \text{ mL}$ ;  $m(\text{catalyst}) = 100 \text{ mg}$ ;  $t = 3 \text{ h}$ ;  $T = 65 \text{ °C}$ ; under a  $\text{N}_2$  atmosphere]. (C) XRD patterns of the spent catalyst run-by-run. (D) Short scope of the catalytic system [main products are depicted in the order of furfuryl alcohol; cinnamyl alcohol, crotyl alcohol; benzyl alcohol; 1-phenylethanol, cyclohexanol. Reaction time: 8 h except for cyclohexanol (2 h)].

were leached into the reaction mixture and the catalysts used were a true heterogeneous catalyst.

The stability and recyclability of the catalyst were investigated by separating, washing, and reusing the spent catalyst after the successful MPV reduction under the optimized reaction conditions (except for the used reaction time: 1 h). The data presented in Figure 9B clearly show that the cyclohexanol yield remained constant in three consecutive runs and decreased by 5–10% overall in the fourth and fifth runs. No further decrease in activity was observed during further recycling. Remarkably, there were no changes in the unique selectivity of the catalyst during the recycling tests. By performing an ex-situ XRD study of the spent catalyst after different runs, a plausible explanation for the loss of activity in the corresponding runs was found (Figure 9C). After the fourth run, a characteristic reflection of  $\text{CeO}_2$  was observed in the corresponding diffractogram, which increased in intensity in the spent sample used in the fifth run. However, the intensity ratios between the LDH reflections and the  $\text{CeO}_2$  reflections became constant in the spent samples after the fifth run, in parallel with the restabilization of the cyclohexanol yields.

The remarkable activity of  $\text{MgAlCe}_{0.075}$  pretreated at 200 °C has encouraged us to extend our study to LDH-catalyzed MPV reductions of some other industrially important biomass-derived ketones and aldehydes (Figure 9D, S14, and Table S2). In these cases, a moderate-to-high conversion of carbonyl compounds was achieved within 8 h (2 h in the case of cyclohexanol) at different temperatures, depending on the quality of the reactants (Figure S14). In fact, the reaction

**Scheme 2. Proposed Mechanism of the Transfer Hydrogenation of Cyclohexanone to Cyclohexanol in 2-Propanol Catalyzed by the  $\text{MgAlCe}_{0.075}$  Catalyst**



temperature plays a crucial role due to the Brønsted/Lewis base property of the LDH framework. If a higher temperature was applied to promote the reaction, aldol condensation occurred as an undesirable side reaction, which reduced alcohol selectivity. Excitedly, the yield and selectivity seem to be competitive or even superior to the best available technologies to prepare the above listed biomass derived alcohols in these cases,<sup>11</sup> demonstrating the versatility of the optimized catalyst, i.e.,  $\text{MgAlCe}_{0.075}$ , for MPV reductions.

**Mechanistic Insight of the  $\text{MgAlCe}_{0.075}$  Catalyzed MPV Reduction of Cyclohexanone.** In order to propose an appropriate reaction mechanism, some control experiments were performed focusing on the catalytic ability of  $\text{MgAlCe}_{0.075}$  and its building blocks for oxidation/oxidative-dehydrogenative transformations of alcohols (benzyl alcohol, 1,2-hexanediol, and diphenylmethanol) (Scheme S2 and Table S5). This is the rate-determining step of the MPV mechanism. As can be seen, neither pure LDH nor its partially dehydrated counterpart can promote these transformations, highlighting their negligible role in these reactions. When cerium-containing catalysts were used, all of them catalyzed the conversion of alcohols except diol, as its oxidation is less favorable than that of primary or even secondary alcohols (Table S5, rows 1–3). In sharp contrast, when the tests were repeated under a  $\text{N}_2$  atmosphere, only hydrated nanoceria with surface defect sites and hydroxyl groups as well as FLP-containing  $\text{CeO}_2$  proved to be active catalysts (Table S5, rows 4–6). In addition, the same trend was observed in the presence of an acceptor molecule (aniline, Table S5, rows 7–9), using an  $\text{N}_2$  atmosphere. This means that in the case of a Ce-containing catalyst, the presence of an FLP-like structure<sup>27</sup> and/or Ce(III) centers surrounded by hydroxyl functions<sup>71</sup> are probably necessary in the dehydrogenation of alcohols under an inert atmosphere where Ce(IV) oxide-type catalysts are very inactive as is well-known based on the literature data.<sup>72</sup> The best performance can be achieved when Ce(III) centers, hydroxyl groups with basic character, and defect sites are

simultaneously present on the active surface (hydrated nanoceria). When the  $\text{MgAlCe}_{0.075}$  catalyst was included in these test reactions, it was found that its performance exceeded that of all Ce-containing (and also LDH-containing) catalysts and only the hydrated nanoceria could match its efficiency. Thus, similar active centers are found in both catalysts, but in  $\text{MgAlCe}_{0.075}$ , the cerium centers are (possibly) much more isolated than those in hydrated nanoceria.

Based on all this information, a likely reaction mechanism for the Ce-LDH-catalyzed MPV reduction of cyclohexanone was proposed (Scheme 2), considering the results reported for high entropy oxides<sup>28</sup> with FLP-like activity in combination with the classical acid–base mechanism.<sup>7</sup> Accordingly, in the first step, the dissociative adsorption of the 2-propanol molecule onto a coordinatively unsaturated Ce(III) center takes place with the help of the framework –OH unit with Lewis basic character. This first step is supported by three facts. First, in most coordination compounds of cerium cations, the coordination number is between 7 and 9, so both Ce(III) and Ce(IV) in the LDH structure can be treated as coordinatively unsaturated centers,<sup>73</sup> but are stabilized by the LDH lattice. Second, methanol adsorption studies have shown that the MgAl-LDH surface can adsorb alcohol molecules in a dissociative manner. Finally, through the control experiments, a catalyst having Ce(III)-containing centers in conjunction with the hydroxyl functions exhibited notable performance for promoting dehydrogenation of alcohols. The main role of Ce(III) centers in this step can be also supposed according to the comparative study of alcohol oxidations catalyzed by highly active Ce(III) complexes, which has also declared the reduced activity of Ce(IV) complexes.<sup>74</sup> In the absence of Ce(III) centers, this step can also take place at Ce(IV) centers but with a low efficiency. In the second step, the electron-rich oxygen of the carbonyl group of cyclohexanone coordinates to an electron-deficient –OH vacancy with Lewis acidic features similar to a key step previously proposed for FLP-like surfaces. Then in the third step, similar to the classical MPV

mechanism, the formation of a six-membered ring intermediate occurs, immediately followed by the transfer of both  $\alpha$ -H and hydrogen of the OH group of the alcohol molecule to the carbonyl group in a concerted step. Finally in steps 4 and 5, desorption of the products (cyclohexanol, acetone) occurs, which also regenerates the active sites on the surface for the subsequent reactions.

## CONCLUSIONS

In conclusion, cerium-containing LDH can act as highly efficient heterogeneous catalysts to promote the MPV reduction of various ketones and aldehydes. Highly crystalline phase-pure Ce-containing LDHs ( $\text{Mg}_3\text{Al}_{1-x}\text{Ce}_x\text{-LDH}$ ) were prepared by using modified coprecipitation processes. In contrast to the previously reported synthesis, our method allowed the preparation of phase-pure Ce-LDHs, but with a severe limitation on the maximum amount of incorporated cerium centers (actual ratio of  $\sim 11\%$  of the total M(III) cations). By adopting a very broad characterization (XRD, TG/DTG, ICP-AES, FT-IR, BET, SEM, DLS, FLS, XPS, SS-NMR, and Raman), it was clearly demonstrated that Ce incorporation was successful, and both Ce(III) and Ce(IV) centers were formed in the LDH lattice. Interestingly, the Ce(III)/Ce(IV) ratios were found to increase with the Ce loading amount up to 7.5% and then decrease with the Ce loading amount to 11%. The incorporation of cerium centers into LDHs was accompanied by the formation of surface/subsurface defects, e.g., tetrahedrally coordinated aluminum centers. As a result of cerium incorporation, the Lewis acidity of LDHs was greatly increased in parallel with slight changes in the basic properties of LDHs. The as-prepared and subsequently heat-treated ( $T = 200\text{ }^\circ\text{C}$ )  $\text{MgAlCe}_{0.075}$  showed remarkable catalytic performance in the selective MPV reduction of cyclohexanone (45% cyclohexanol yield) under the optimized and mild reaction conditions ( $m(\text{catalyst}) = 100\text{ mg}$ ;  $V(\text{IPA}) = 3\text{ mL}$ ;  $T = 65\text{ }^\circ\text{C}$ ;  $t = 3\text{ h}$ ). The catalytic activity of these systems was strongly dependent on the amount of Ce(III) centers as well as Ce(IV) centers. Moreover, the crucial role of the hydroxyl group on the surface was demonstrated, and a strongly enhanced catalytic activity of these structures was observed in the presence of surface or subsurface defect sites (such as tetrahedral aluminum cations), indicating solid FLP-like catalytic behavior. Heterogeneity, recyclability, and versatility of these systems were demonstrated, further showing the high activity of  $\text{MgAlCe}_{0.075}$  in the reduction of chosen, biomass-derived aldehydes and ketones, with the catalytic performance comparable or even superior to the benchmark catalysts.

## ASSOCIATED CONTENT

### Supporting Information

The Supporting Information is available free of charge at <https://pubs.acs.org/doi/10.1021/acsami.3c16732>.

Detailed experimental part; representative BET isotherms; representative SEM images, ATR-FTIR spectrum of carbonate modified structure, XRD patterns of the heat-treated and nonphase pure structures, representative TG/DTG curves,  $\text{O}_2$ -/ $\text{CO}_2$ -/ $\text{NH}_3$ -TPD curves, optimization procedure of MPV reaction of aldehydes and acetophenone, and XP and FTIR spectra of the modified structures and the control experiments (PDF)

## AUTHOR INFORMATION

### Corresponding Authors

**Gábor Varga** – Australian Institute for Bioengineering and Nanotechnology, The University of Queensland, Queensland 4072, Australia; Interdisciplinary Excellence Centre, Department of Applied and Environmental Chemistry, University of Szeged, Szeged H-6720, Hungary; [orcid.org/0000-0002-7131-1629](https://orcid.org/0000-0002-7131-1629); Email: [gabor.varga5@chem.u-szeged.hu](mailto:gabor.varga5@chem.u-szeged.hu)

**Zhi Ping Xu** – Australian Institute for Bioengineering and Nanotechnology, The University of Queensland, Queensland 4072, Australia; [orcid.org/0000-0001-6070-5035](https://orcid.org/0000-0001-6070-5035); Email: [gordonxu@uq.edu.au](mailto:gordonxu@uq.edu.au)

### Authors

**Thanh-Truc Nguyen** – Australian Institute for Bioengineering and Nanotechnology, The University of Queensland, Queensland 4072, Australia

**Jing Wang** – Key Laboratory of OptoElectronic Science and Technology for Medicine of Ministry of Education, Fujian Provincial Key Laboratory of Photonics Technology, Fujian Normal University, Fuzhou 350117, China; [orcid.org/0000-0001-6080-7998](https://orcid.org/0000-0001-6080-7998)

**Dihua Tian** – Australian Institute for Bioengineering and Nanotechnology, The University of Queensland, Queensland 4072, Australia

**Run Zhang** – Australian Institute for Bioengineering and Nanotechnology, The University of Queensland, Queensland 4072, Australia; [orcid.org/0000-0002-0943-824X](https://orcid.org/0000-0002-0943-824X)

**Li Li** – Australian Institute for Bioengineering and Nanotechnology, The University of Queensland, Queensland 4072, Australia; [orcid.org/0000-0001-6545-858X](https://orcid.org/0000-0001-6545-858X)

Complete contact information is available at: <https://pubs.acs.org/10.1021/acsami.3c16732>

### Author Contributions

The manuscript was written through contributions of all authors. All authors have given approval to the final version of the manuscript.

### Notes

The authors declare no competing financial interest.

## ACKNOWLEDGMENTS

This project has received funding from the European Union's Horizon 2020 research and innovation programme under grant agreement no. 101030066 (Marie Skłodowska-Curie Global Fellowship). Facilities and assistance of the Australian Microscopy & Microanalysis Research Facility at the Centre for Microscopy and Microanalysis (CMM), Queensland node of the NCRIS-enabled Australian National Fabrication Facility (ANFF-Q), and Centre of Advance Imaging (CAI), The University of Queensland, are also acknowledged. One of us, T.-T.N. thanks for the Vingroup Science and Technology Scholarship Program for Overseas Study for Master's and Doctoral Degrees for sponsoring the opportunity to pursue her degree at UQ. The financial helps are highly appreciated. This work was also supported by the University of Szeged Open Access Fund (Grant number: 6841).

## REFERENCES

- (1) Magano, J.; Dunetz, J. R. Large-Scale Carbonyl Reductions in the Pharmaceutical Industry. *Org. Process Res. Dev.* **2012**, *16* (6), 1156–1184.
- (2) Caron, S.; Dugger, R. W.; Ruggeri, S. G.; Ragan, J. A.; Ripin, D. H. B. Large-Scale Oxidations in the Pharmaceutical Industry. *Chem. Rev.* **2006**, *106* (7), 2943–2989.
- (3) He, M.; Sun, Y.; Han, B. Green Carbon Science: Efficient Carbon Resource Processing, Utilization, and Recycling towards Carbon Neutrality. *Angew. Chem., Int. Ed.* **2022**, *61* (15), No. e202112835.
- (4) Burns, N. Z.; Baran, P. S.; Hoffmann, R. W. Redox Economy in Organic Synthesis. *Angew. Chem., Int. Ed.* **2009**, *48* (16), 2854–2867.
- (5) Wang, D.; Astruc, D. The Golden Age of Transfer Hydrogenation. *Chem. Rev.* **2015**, *115* (13), 6621–6686.
- (6) Sudarsanam, P.; Zhong, R.; Van Den Bosch, S.; Coman, S. M.; Parvulescu, V. I.; Sels, B. F. Functionalised Heterogeneous Catalysts for Sustainable Biomass Valorisation. *Chem. Soc. Rev.* **2018**, *47* (22), 8349–8402.
- (7) Li, A. Y.; Moores, A. Carbonyl Reduction and Biomass: A Case Study of Sustainable Catalysis. *ACS Sustain. Chem. Eng.* **2019**, *7* (12), 10182–10197.
- (8) Hao, H.; Abe, Y.; Guo, H.; Zhang, X.; Lee Smith, R. Catalytic Transfer Hydrogenation and Ethanolysis of Furfural to Ethyl Levulinate Using Sulfonated Hf- or Ni-Catalysts Prepared with Mixed Solvents. *ACS Sustain. Chem. Eng.* **2022**, *10* (49), 16261–16270.
- (9) Fang, W.; Riisager, A. Improved Catalytic Transfer Hydrogenation of Biomass-Derived Aldehydes with Metal-Loaded Aluminum Phosphate. *ACS Sustain. Chem. Eng.* **2022**, *10* (4), 1536–1543.
- (10) Gilkey, M. J.; Xu, B. Heterogeneous Catalytic Transfer Hydrogenation as an Effective Pathway in Biomass Upgrading. *ACS Catal.* **2016**, *6* (3), 1420–1436.
- (11) Kumar, A.; Bhardwaj, R.; Mandal, S. K.; Choudhury, J. Transfer Hydrogenation of CO<sub>2</sub> and CO<sub>2</sub> Derivatives Using Alcohols as Hydride Sources: Boosting an H<sub>2</sub>-Free Alternative Strategy. *ACS Catal.* **2022**, *12* (15), 8886–8903.
- (12) Shao, Y. R.; Zhao, F.; Wei, Z. C.; Huo, Y. F.; Dai, J. J.; Hu, T. L. Confining Co-Based Nanocatalysts by Ultrathin Nanotubes for Efficient Transfer Hydrogenation of Biomass Derivatives. *ACS Appl. Mater. Interfaces* **2023**, *15* (22), 26637–26649.
- (13) Török, B.; Schafer, C.; Kokel, A. *Heterogeneous Catalysis in Sustainable Synthesis*; Elsevier: Cambridge, Oxford, 2022.
- (14) Samec, J. S. M.; Bäckvall, J. E.; Andersson, P. G.; Brandt, P. Mechanistic Aspects of Transition Metal-Catalyzed Hydrogen Transfer Reactions. *Chem. Soc. Rev.* **2006**, *35* (3), 237–248.
- (15) Luo, H. Y.; Consoli, D. F.; Gunther, W. R.; Román-Leshkov, Y. Investigation of the Reaction Kinetics of Isolated Lewis Acid Sites in Beta Zeolites for the Meerwein-Ponndorf-Verley Reduction of Methyl Levulinate to  $\gamma$ -Valerolactone. *J. Catal.* **2014**, *320* (1), 198–207.
- (16) Muhammad, A.; Zhu, C.; Yu, X.; Di Carmine, G.; Wood, H.; Carbone, P.; de Visser, S. P.; Hardacre, C.; D'Agostino, C. Heterogenised Catalysts for the H-Transfer Reduction Reaction of Aldehydes: Influence of Solvent and Solvation Effects on Reaction Performances. *Phys. Chem. Chem. Phys.* **2023**, *25*, 21416–21427.
- (17) Zhang, H.; Samsudin, I. b.; Jaenicke, S.; Chuah, G. K. Zeolites in Catalysis: Sustainable Synthesis and Its Impact on Properties and Applications. *Catal. Sci. Technol.* **2022**, *12* (19), 6024–6039.
- (18) Boronat, M.; Corma, A.; Renz, M. Mechanism of the Meerwein-Ponndorf-Verley-Oppenauer (MPVO) Redox Equilibrium on Sn- and Zr-Beta Zeolite Catalysts. *J. Phys. Chem. B* **2006**, *110* (42), 21168–21174.
- (19) Corma, A.; Domine, M. E.; Valencia, S. Water-Resistant Solid Lewis Acid Catalysts: Meerwein-Ponndorf-Verley and Oppenauer Reactions Catalyzed by Tin-Beta Zeolite. *J. Catal.* **2003**, *215* (2), 294–304.
- (20) Di Iorio, J. R.; Johnson, B. A.; Román-Leshkov, Y. Ordered Hydrogen-Bonded Alcohol Networks Confined in Lewis Acid Zeolites Accelerate Transfer Hydrogenation Turnover Rates. *J. Am. Chem. Soc.* **2020**, *142* (45), 19379–19392.
- (21) Song, J.; Hua, M.; Huang, X.; Visa, A.; Wu, T.; Fan, H.; Hou, M.; Zhang, Z.; Han, B. Highly Efficient Meerwein-Ponndorf-Verley Reductions over a Robust Zirconium-Organoboronic Acid Hybrid. *Green Chem.* **2021**, *23* (3), 1259–1265.
- (22) Gonell, F.; Boronat, M.; Corma, A. Structure-Reactivity Relationship in Isolated Zr Sites Present in Zr-Zeolite and ZrO<sub>2</sub> for the Meerwein-Ponndorf-Verley Reaction. *Catal. Sci. Technol.* **2017**, *7* (13), 2865–2873.
- (23) Yang, X.; Yuan, Z.; Zhou, M.; Chen, F.; Xu, B.; Shi, H. Toward a Better Understanding of Intrinsic Activity Trends in Zr-Based Heterogeneous Catalysts for Meerwein-Ponndorf-Verley Reduction of Levulinic Esters. *ACS Catal.* **2023**, *13*, 10953–10967.
- (24) Stephan, D. W. Catalysis, FLPs, and Beyond. *Chem* **2020**, *6* (7), 1520–1526.
- (25) Ma, Y.; Zhang, S.; Chang, C. R.; Huang, Z. Q.; Ho, J. C.; Qu, Y. Semi-Solid and Solid Frustrated Lewis Pair Catalysts. *Chem. Soc. Rev.* **2018**, *47* (15), 5541–5553.
- (26) Zhang, S.; Huang, Z. Q.; Ma, Y.; Gao, W.; Li, J.; Cao, F.; Li, L.; Chang, C. R.; Qu, Y. Solid Frustrated-Lewis-Pair Catalysts Constructed by Regulations on Surface Defects of Porous Nanorods of CeO<sub>2</sub>. *Nat. Commun.* **2017**, *8* (1), 15266.
- (27) Zou, Y.; Zhang, M.; Liu, Y.; Ma, Y.; Zhang, S.; Qu, Y. Highly Selective Transfer Hydrogenation of Furfural into Furfuryl Alcohol by Interfacial Frustrated Lewis Pairs on CeO<sub>2</sub>. *J. Catal.* **2022**, *410*, 54–62.
- (28) Ma, M.; Li, L.; Tian, G.; Geng, Z.; Zhang, X.; Zhao, X.; Li, G. Creation of Surface Frustrated Lewis Pairs on High-Entropy Spinel Nanocrystals That Boosts Catalytic Transfer Hydrogenation Reaction. *Chem. Eng. J.* **2023**, *470* (April), 144291.
- (29) Pütz, E.; Smales, G. J.; Jegel, O.; Emmerling, F.; Tremel, W. Tuning Ceria Catalysts in Aqueous Media at the Nanoscale: How Do Surface Charge and Surface Defects Determine Peroxidase- and Haloperoxidase-like Reactivity. *Nanoscale* **2022**, *14* (37), 13639–13650.
- (30) Gu, Z.; Atherton, J. J.; Xu, Z. P. Hierarchical Layered Double Hydroxide Nanocomposites: Structure, Synthesis and Applications. *Chem. Commun.* **2015**, *51* (15), 3024–3036.
- (31) Xu, Z. P.; Lu, G. Q. M. Hydrothermal Synthesis of Layered Double Hydroxides (LDHs) from Mixed MgO and Al<sub>2</sub>O<sub>3</sub>: LDH Formation Mechanism. *Chem. Mater.* **2005**, *17* (5), 1055–1062.
- (32) Karádi, K.; Nguyen, T. T.; Ádám, A. A.; Baán, K.; Sápi, A.; Kukovec, Á.; Kónya, Z.; Sipos, P.; Pálincó, I.; Varga, G. Structure-Activity Relationships of LDH Catalysts for the Glucose-to-Fructose Isomerisation in Ethanol. *Green Chem.* **2023**, *25*, 5741–5755.
- (33) Pálincó, I.; Sipos, P.; Berkesi, O.; Varga, G. Distinguishing Anionic Species That Are Intercalated in Layered Double Hydroxides from Those Bound to Their Surface: A Comparative IR Study. *J. Phys. Chem. C* **2022**, *126* (36), 15254–15262.
- (34) Varga, G.; Kukovec, Á.; Kónya, Z.; Korecz, L.; Muráth, S.; Csendes, Z.; Peintler, G.; Carlson, S.; Sipos, P.; Pálincó, I. Mn(II)-Amino Acid Complexes Intercalated in CaAl-Layered Double Hydroxide - Well-Characterized, Highly Efficient, Recyclable Oxidation Catalysts. *J. Catal.* **2016**, *335*, 125–134.
- (35) Li, B.; Gu, Z.; Kurniawan, N.; Chen, W.; Xu, Z. P. Manganese-Based Layered Double Hydroxide Nanoparticles as a T1-MRI Contrast Agent with Ultrasensitive PH Response and High Relaxivity. *Adv. Mater.* **2017**, *29* (29), 1700373.
- (36) Liu, J.; Sun, L.; Li, L.; Zhang, R.; Xu, Z. P. Synergistic Cancer Phototherapy via Layered Double Hydroxide-Based Trimodal Nanomedicine at Very Low Therapeutic Doses. *ACS Appl. Mater. Interfaces* **2021**, *13* (6), 7115–7126.
- (37) Varga, G.; Somosi, Z.; Kónya, Z.; Kukovec, Á.; Pálincó, I.; Szilágyi, I. A Colloid Chemistry Route for the Preparation of Hierarchically Ordered Mesoporous Layered Double Hydroxides Using Surfactants as Sacrificial Templates. *J. Colloid Interface Sci.* **2021**, *581*, 928–938.

- (38) Smalenskaite, A.; Vieira, D. E. L.; Salak, A. N.; Ferreira, M. G. S.; Katselnykova, A.; Kareiva, A. A Comparative Study of Co-Precipitation and Sol-Gel Synthetic Approaches to Fabricate Cerium-Substituted Mg-Al Layered Double Hydroxides with Luminescence Properties. *Appl. Clay Sci.* **2017**, *143* (December 2016), 175–183.
- (39) Wang, Z.; Fongarland, P.; Lu, G.; Essayem, N. Reconstructed La-Y-Ce-Modified MgAl-Hydrotalcite as a Solid Base Catalyst for Aldol Condensation: Investigation of Water Tolerance. *J. Catal.* **2014**, *318*, 108–118.
- (40) Labajos, F. M.; Sastre, M. D.; Trujillano, R.; Rives, V. New Layered Double Hydroxides with the Hydrotalcite Structure Containing Ni(II) and V(III). *J. Mater. Chem.* **1999**, *9* (4), 1033–1039.
- (41) Liu, J.; Li, L.; Zhang, R.; Xu, Z. P. The Adjacent Effect between Gd(III) and Cu(II) in Layered Double Hydroxide Nanoparticles Synergistically Enhances T1-Weighted Magnetic Resonance Imaging Contrast. *Nanoscale Horiz.* **2023**, *8* (2), 279–290.
- (42) Hidalgo, J. M.; Jiménez-Sanchidrián, C.; Ruiz, J. R. Delaminated Layered Double Hydroxides as Catalysts for the Meerwein-Ponndorf-Verley Reaction. *Appl. Catal., A* **2014**, *470*, 311–317.
- (43) Bing, W.; Zheng, L.; He, S.; Rao, D.; Xu, M.; Zheng, L.; Wang, B.; Wang, Y.; Wei, M. Insights on Active Sites of CaAl-Hydrotalcite as a High-Performance Solid Base Catalyst toward Aldol Condensation. *ACS Catal.* **2018**, *8* (1), 656–664.
- (44) Xiao, Z. Insight into the Meerwein-Ponndorf-Verley Reduction of Cinnamaldehyde over MgAl Oxides Catalysts. *Mol. Catal.* **2017**, *436*, 1–9.
- (45) Kumbhar, P. S.; Sanchez-Valente, J.; Lopez, J.; Figueras, F. Meerwein-Ponndorf-Verley Reduction of Carbonyl Compounds Catalysed by Mg-Al Hydrotalcite. *Chem. Commun.* **1998**, No. 5, 535–536.
- (46) Komanoya, T.; Nakajima, K.; Kitano, M.; Hara, M. Synergistic Catalysis by Lewis Acid and Base Sites on ZrO<sub>2</sub> for Meerwein-Ponndorf-Verley Reduction. *J. Phys. Chem. C* **2015**, *119* (47), 26540–26546.
- (47) Lin, Y. J.; Li, D. Q.; Evans, D. G.; Duan, X. Modulating Effect of Mg-Al-CO<sub>3</sub> Layered Double Hydroxides on the Thermal Stability of PVC Resin. *Polym. Degrad. Stab.* **2005**, *88* (2), 286–293.
- (48) Pan, G.; Cheng, S.; Zhang, Y.; Chen, Y.; Xu, X.; Xu, J. In Situ Reduction of Cu Nanoparticles on Mg-Al-LDH for Simultaneous Efficient Catalytic Transfer Hydrogenation of Furfural to Furfuryl Alcohol. *Chem. Commun.* **2023**, *59* (22), 3301–3304.
- (49) Zhang, J.; Su, H.; Zhou, J.; Qian, G.; Xu, Z.; Xi, Y.; Xu, Y.; Theiss, F. L.; Frost, R. Mid- and near-Infrared Spectroscopic Investigation of Homogeneous Cation Distribution in Mg<sub>x</sub>Zn<sub>y</sub>Al<sub>(x+y)/2</sub>-Layered Double Hydroxide (LDH). *J. Colloid Interface Sci.* **2013**, *411*, 240–246.
- (50) Coenen, K.; Gallucci, F.; Mezari, B.; Hensen, E.; van Sint Annaland, M. An In-Situ IR Study on the Adsorption of CO<sub>2</sub> and H<sub>2</sub>O on Hydrotalcites. *J. CO<sub>2</sub> Util.* **2018**, *24* (March), 228–239.
- (51) Bhattacharyya, K.; Danon, A.; K.Vijayan, B.; Gray, K. A.; Stair, P. C.; Weitz, E. Role of the Surface Lewis Acid and Base Sites in the Adsorption of CO<sub>2</sub> on Titania Nanotubes and Platinized Titania Nanotubes: An in Situ FT-IR Study. *J. Phys. Chem. C* **2013**, *117* (24), 12661–12678.
- (52) Matthews, R. W.; Sworski, T. J. Photooxidation and Fluorescence of Cerium(III) in Aqueous Sulfuric Acid Solutions. *J. Phys. Chem.* **1975**, *79* (7), 681–686.
- (53) Yang, Z.; Wang, X.; Qin, W.; Zhao, H. Capillary Electrophoresis-Chemiluminescence Determination of Norfloxacin and Prulifloxacin. *Anal. Chim. Acta* **2008**, *623* (2), 231–237.
- (54) Larachi, F.; Pierre, J.; Adnot, A.; Bernis, A. Ce 3d XPS Study of Composite Ce<sub>x</sub>Mn<sub>1-x</sub>O<sub>2-y</sub> Wet Oxidation Catalysts. *Appl. Surf. Sci.* **2002**, *195* (1–4), 236–250.
- (55) Valente, J. S.; Lima, E.; Toledo-Antonio, J. A.; Cortes-Jacome, M. A.; Lartundo-Rojas, L.; Montiel, R.; Prince, J. Comprehending the Thermal Decomposition and Reconstruction Process of Sol-Gel MgAl Layered Double Hydroxides. *J. Phys. Chem. C* **2010**, *114* (5), 2089–2099.
- (56) Willis, S. A.; McGuinness, E. K.; Li, Y.; Losego, M. D. Re-Examination of the Aqueous Stability of Atomic Layer Deposited (ALD) Amorphous Alumina (Al<sub>2</sub>O<sub>3</sub>) Thin Films and the Use of a Postdeposition Air Plasma Anneal to Enhance Stability. *Langmuir* **2021**, *37* (49), 14509–14519.
- (57) Li, B.; Yang, Z.; Dou, Y.; Zhang, J.; Lu, J.; Han, J. Two-Dimensional LDH Film Templating for Controlled Preparation and Performance Enhancement of Polyamide Nanofiltration Membranes. *Angew. Chem., Int. Ed.* **2023**, *62*, No. e202304442.
- (58) Vyalikh, A.; Costa, F. R.; Wagenknecht, U.; Heinrich, G.; Massiot, D.; Scheler, U. From Layered Double Hydroxides to Layered Double Hydroxide-Based Nanocomposites - A Solid-State NMR Study. *J. Phys. Chem. C* **2009**, *113* (51), 21308–21313.
- (59) Schilling, C.; Hofmann, A.; Hess, C.; Ganduglia-Pirovano, M. V. Raman Spectra of Polycrystalline CeO<sub>2</sub>: A Density Functional Theory Study. *J. Phys. Chem. C* **2017**, *121* (38), 20834–20849.
- (60) Xu, Y.; Wang, F.; Liu, X.; Liu, Y.; Luo, M.; Teng, B.; Fan, M.; Liu, X. Resolving a Decade-Long Question of Oxygen Defects in Raman Spectra of Ceria-Based Catalysts at Atomic Level. *J. Phys. Chem. C* **2019**, *123* (31), 18889–18894.
- (61) Theiss, F.; López, A.; Frost, R. L.; Scholz, R. Spectroscopic Characterisation of the LDH Mineral Quintinite Mg<sub>4</sub>Al<sub>2</sub>(OH)<sub>12</sub>CO<sub>3</sub>·3H<sub>2</sub>O. *Spectrochim. Acta, Part A* **2015**, *150*, 758–764.
- (62) Rudolph, W. W.; Irmer, G. Raman Spectroscopic Characterization of Light Rare Earth Ions: La<sup>3+</sup>, Ce<sup>3+</sup>, Pr<sup>3+</sup>, Nd<sup>3+</sup> and Sm<sup>3+</sup> - Hydration and Ion Pair Formation. *Dalton Trans.* **2017**, *46* (13), 4235–4244.
- (63) Jiang, B.; Xi, Z.; Lu, F.; Huang, Z.; Yang, Y.; Sun, J.; Liao, Z.; Wang, J.; Yang, Y. Ce/MgAl Mixed Oxides Derived from Hydrotalcite LDH Precursors as Highly Efficient Catalysts for Ketonization of Carboxylic Acid. *Catal. Sci. Technol.* **2019**, *9* (22), 6335–6344.
- (64) Chisem, I. C.; Jones, W.; Martín, I.; Martín, C.; Rives, V. Probing the Surface Acidity of Lithium Aluminium and Magnesium Aluminium Layered Double Hydroxides. *J. Mater. Chem.* **1998**, *8* (8), 1917–1925.
- (65) Navajas, A.; Arzamendi, G.; Romero-Sarria, F.; Centeno, M. A.; Odriozola, J. A.; Gandía, L. DRIFTS Study of Methanol Adsorption on Mg-Al Hydrotalcite Catalysts for the Transesterification of Vegetable Oils. *Catal. Commun.* **2012**, *17*, 189–193.
- (66) Lei, X.; Zhang, F.; Yang, L.; Guo, X.; Tian, Y.; Fu, S.; Li, F.; Evans, D. G.; Duan, X. Highly Crystalline Activated Layered Double Hydroxides as Solid Acid-Base Catalysts. *AIChE J.* **2007**, *53* (4), 932–940.
- (67) Ferreira, S. L. C.; Bruns, R. E.; Ferreira, H. S.; Matos, G. D.; David, J. M.; Brandão, G.; da Silva, E. G. P.; Portugal, L. A.; dos Reis, P. S.; Souza, A. S.; dos Santos, W. N. L. Box-Behnken Design: An Alternative for the Optimization of Analytical Methods. *Anal. Chim. Acta* **2007**, *597* (2), 179–186.
- (68) Bock, L.; Tran, X.; Liang, Y.; Kramer, M.; Maichle-Mössmer, C.; Anwender, R. SOMC@Periodic Mesoporous Silica Nanoparticles: Meerwein-Ponndorf-Verley Reduction Promoted by Immobilized Rare-Earth-Metal Alkoxides. *Organometallics* **2020**, *39* (7), 1046–1058.
- (69) Suo, H.; Duan, H.; Chen, C.; Buffet, J. C.; O'Hare, D. Bifunctional Acid-Base Mesoporous Silica@aqueous Miscible Organic-Layered Double Hydroxides. *RSC Adv.* **2019**, *9* (7), 3749–3754.
- (70) Valente, J. S.; Hernandez-Cortez, J.; Cantu, M. S.; Ferrat, G.; López-Salinas, E. Calcinated Layered Double Hydroxides Mg-Me-Al (Me: Cu, Fe, Ni, Zn) as Bifunctional Catalysts. *Catal. Today* **2010**, *150* (3–4), 340–345.
- (71) Bourja, L.; Bakiz, B.; Benhachemi, A.; Ezahri, M.; Villain, S.; Favotto, C.; Valmalette, J. C.; Gavarri, J. R. Structural Modifications of Nanostructured Ceria CeO<sub>2</sub>·xH<sub>2</sub>O during Dehydration Process. *Powder Technol.* **2012**, *215–216*, 66–71.
- (72) Zhang, M.; Wu, S.; Bian, L.; Cao, Q.; Fang, W. One-Pot Synthesis of Pd-Promoted Ce-Ni Mixed Oxides as Efficient Catalysts

for Imine Production from the Direct: N -Alkylation of Amine with Alcohol. *Catal. Sci. Technol.* **2019**, *9* (2), 286–301.

(73) Farahmand Kateshali, A.; Gholizadeh Dogaheh, S.; Soleimannejad, J.; Blake, A. J. Structural Diversity and Applications of Ce(III)-Based Coordination Polymers. *Coord. Chem. Rev.* **2020**, *419*, 213392.

(74) Tsurugi, H.; Mashima, K. Renaissance of Homogeneous Cerium Catalysts with Unique Ce(IV/III) Couple: Redox-Mediated Organic Transformations Involving Homolysis of Ce(IV)-Ligand Covalent Bonds. *J. Am. Chem. Soc.* **2021**, *143* (21), 7879–7890.